Application of Polarizing Optical Microscopy in Investigation of Crystallization Kinetics from Smectic C_A^* Phase

A. Deptuch[a,*], A. Lelito[b] and M. Urbańska[c]

[a] *Institute of Nuclear Physics, Polish Academy of Sciences, Radzikowskiego 152, PL-31342 Kraków, Poland*
[b] *Faculty of Materials Engineering and Physics, Cracow University of Technology, PL-30084 Kraków, Poland*
[c] *Institute of Chemistry, Military University of Technology, Kaliskiego 2, PL-00908 Warsaw, Poland*

Received: 09.05.2023 & Accepted: 30.06.2023

Doi: 10.12693/APhysPolA.144.93 *e-mail: aleksandra.deptuch@ifj.edu.pl

Polarizing optical microscopy is used to investigate the isothermal and non-isothermal crystallization of the 3F6FPhF6 compound, which exhibits the smectic C^* and smectic C_A^* phases. A large hysteresis of above 20 K in the smectic C^*/smectic C_A^* phase transition is reported. The kinetics of non-isothermal crystallization is analyzed by means of the continuous cooling transition diagram. The cooling rate necessary for at least partial vitrification of the smectic C_A^* phase is estimated. The relationship between the thermodynamic driving force of crystallization and thermal energy of the translational degrees of freedom is shown to have a strong impact on crystallization.

topics: liquid crystals, smectic C_A^* phase, crystallization kinetics, polarizing optical microscopy

1. Introduction

Polarizing optical microscopy (POM) is an experimental method frequently applied in the investigation of liquid crystals, which also includes the study of the kinetics of their crystallization [1–8]. The fraction of the crystal phase as a function of time or temperature can be obtained as an area of the POM texture covered by the crystal phase. Moreover, the POM method enables the study of the nucleation process, as the number of nuclei in an observed area can also be determined from the textures, as long as the size of separate nuclei is not too small. It is important to understand the relationship between the crystallization kinetics and molecular structure of liquid crystals, as for practical use, one looks for compounds that are unlikely to crystallize. For the 3FmFPhF6 homologous series (Fig. 1), changes in the length of the -C_mH_{2m}- chain have a significant impact on the tendency to crystallization. The homologue with $m = 5$ crystallizes upon slow cooling [9], but during faster cooling with the rate of at least 10 K/min, it forms the glass of the anticlinic smectic C_A^* phase [8]. Meanwhile, for $m = 4$ [6] and 7 [10], even the fast cooling at 20 K/min leads to crystallization.

2. Experimental details

The synthetic route of the (S)-4'-(1-methylheptyloxycarbonyl)biphenyl-4-yl 4-[6-(2,2,3,3,4,4,4-heptafluorobutoxy)hexyl-1-oxy]-2,3-difluorobenzoate compound, denoted as 3F6FPhF6, is described in [13, 14]. The POM observations were carried out with the Leica microscope for the 3F6FPhF6 sample in the AWAT electro-optic cell with a thickness of 5 μm and with the polymer layer providing planar alignment in the smectic phases. Data analysis was performed in the TOApy [15] and ImageJ [16] programs. The published results for $m = 6$ [11, 12] imply that this homologue is also unlikely to be a glassformer. Nevertheless, the detailed study of crystallization of 3F6FPhF6, presented in this paper, is necessary for comparison with previously studied 3FmFPhF6 homologues with $m = 4$, 5, 7 [6–10].

3. Results and discussion

The POM textures collected during cooling and subsequent heating at the 2 K/min rate were analyzed using the "gray" algorithm of the TOApy

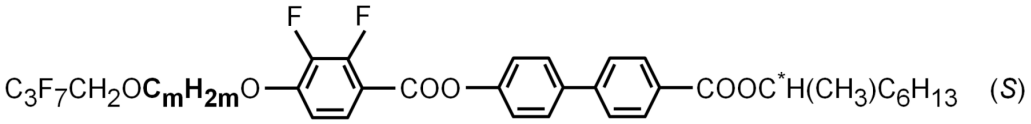

Fig. 1. Molecular formula of the 3FmFPhF6 homologous series.

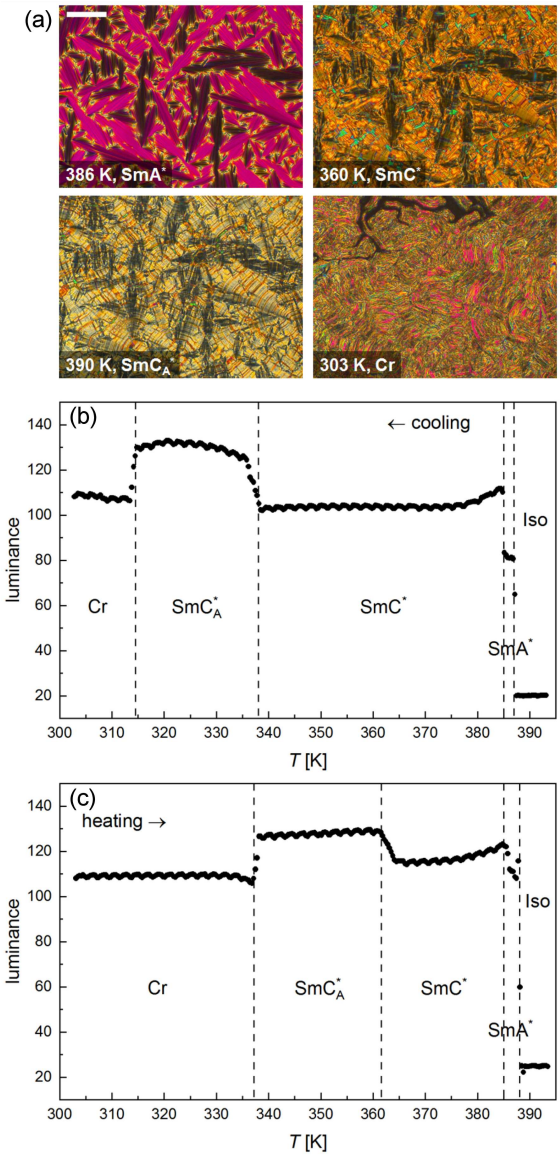

Fig. 2. Selected POM textures collected during cooling at 2 K/min (a) and results of the numerical analysis of POM images for cooling (b) and subsequent heating (c) at 2 K/min. The scale bar denotes 100 μm.

program [15]. In this method of numerical analysis, the textures are converted to grayscale, and the average luminance of all pixels in each texture is calculated. The luminance spans between 0 and 255. The obtained phase sequence is Iso (387 K) SmA* (385 K) SmC* (338 K) SmC$^*_A$ (316 K) Cr during cooling and Cr (337 K) SmC$^*_A$ (361 K) SmC* (385 K) SmA* (388 K) Iso during heating (Fig. 2), where Iso is isotropic liquid, Cr — crystal, and Sm — smectic A*, C*, or C$^*_A$. The measurement has been performed twice, and the average temperatures are given. The differences between the two cooling–heating runs are smaller than 0.5 K. The exception is the temperature of crystallization, which is 314.5 K for the first run and 317.5 K for the second run. Despite the low 2 K/min rate, the SmC*/SmC$^*_A$ and SmC$^*_A$/Cr transitions during cooling are strongly shifted towards lower temperatures compared to results from heating, by 23 K and 21 K, respectively. The supercooling of the SmC$^*_A$ phase below the melting temperature of a crystal is a common observation [5–8], while, to our knowledge, such a strong hysteresis of the transition between SmC* and SmC$^*_A$ was apparently not reported before for compounds with similar molecular structure.

The change of the crystallization degree with time is often described by the Avrami model, which involves such parameters as the initialization time t_0, characteristic crystallization time τ, and the dimensionless n, which depends on the rate of nucleation and shape of crystallites [17–19],

$$X(t) = 1 - \exp\left(-\left(\frac{t-t_0}{\tau}\right)^n\right). \quad (1)$$

The Avrami model is appropriate for crystallization that occurs at constant temperature (isothermal crystallization), although it often describes well the degree of crystallization occurring during the cooling or heating of the sample (non-isothermal crystallization) [20]. In the second case, it can still be used to obtain a reliable interpolation between experimental X values and also to detect changes in the crystallization mechanism [2]. The crystallization rate is obtained by differentiation of (1) over time,

$$\frac{\mathrm{d}X(t)}{\mathrm{d}t} = \frac{n(t-t_0)^{n-1}}{\tau^n}\exp\left(-\left(\frac{t-t_0}{\tau}\right)^n\right). \quad (2)$$

For non-isothermal melt crystallization, $t-t_0$ in (1) and (2) has to be replaced by $(T_0-T)/\phi$, where T_0 is the beginning temperature of crystallization and ϕ is a cooling rate [20]. Therefore,

$$X(T) = 1 - \exp\left(-\left(\frac{T_0-T}{\phi\tau}\right)^n\right), \quad (3)$$

$$\frac{\mathrm{d}X(T)}{\mathrm{d}t} = \frac{n}{\tau^n}\left(\frac{T_0-T}{\phi}\right)^{n-1}\exp\left(-\left(\frac{T_0-T}{\phi\tau}\right)^n\right). \quad (4)$$

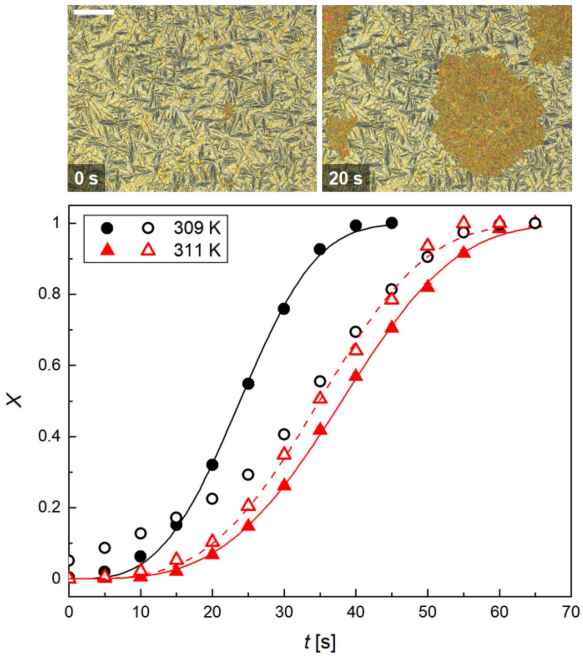

Fig. 3. POM images collected during crystallization in 309 K and degree of crystallization vs time in 309 and 311 K. The uncertainty of crystallization degree is estimated to be 0.01. The scale bar denotes 200 μm.

In some cases, the crystallization process has two stages [21, 22], characterized by different t_0 (or T_0), τ, and n. The overall crystallization degree is then a sum [21]

$$X(t) = AX_1(t) + (1 - A)X_2(t), \tag{5}$$

where A is the fraction of a crystal that develops in the 1st stage of crystallization. As the derivative of a sum is a sum of derivatives, a similar formula can also be applied to the crystallization rate, i.e.,

$$\frac{\mathrm{d}X(t)}{\mathrm{d}t} = A\frac{\mathrm{d}X_1(t)}{\mathrm{d}t} + (1 - A)\frac{\mathrm{d}X_2(t)}{\mathrm{d}t}. \tag{6}$$

In order to investigate the kinetics of crystallization in isothermal conditions, the sample was cooled with the 20 K/min rate from 393 K, i.e., from the isotropic liquid phase to a given temperature T_{cr}, where the POM images were collected every 5 s (Fig. 3). The observation of the isothermal crystallization in various T_{cr} from the 309–315 K range shows that 3F6FPhF6 crystallizes very quickly in these conditions, as the total time of crystallization is 45–195 s. For each temperature, the measurement was performed twice. The number of crystallites in the observed area is small: 3 or 5 in 309 K, 4 in 311 K, and 1–2 in 313, 315 K. When only 1–3 crystallites are visible in the investigated area of the sample, the results may not be representative for the whole sample, therefore only one of the results from 309 K and both from 311 K were analyzed with the Avrami model. The initialization time was set as $t_0 = 0$. The characteristic time equals $\tau = 26.7(2)$ s

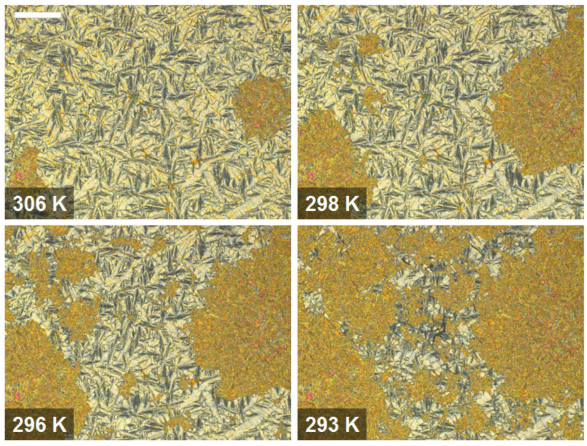

Fig. 4. POM textures during cooling with the 30 K/min rate. The scale bar denotes 200 μm.

in 309 K and 42.3(2) s or 38.8(4) s in 311 K. The exponent n equals 3.3(1) and 3.5(1), 3.4(2) for 309 and 311 K, respectively, which corresponds to isotropic growth of crystals [19].

The beginning of crystallization is already observed after cooling down to 309 K, therefore the isothermal crystallization was not studied for lower temperatures. To investigate the kinetics of crystallization at larger undercooling, non-isothermal POM observations were performed during cooling from 393 K, with the 10–30 K/min rates, until the complete crystallization was visible. For 10, 20, and 30 K/min, the measurement was performed twice. The textures collected during cooling with the 30 K/min rate (Fig. 4) show the two-staged character of crystallization. In the initial stage, the number of observed crystallites N is small and increases to 5 between the beginning of crystallization at ca. 311 K and 301 K. In the texture registered at 298 K, the number of nuclei is already 18, and in the next texture, from 296 K, there are 40 visible nuclei. Eventually, by the end of crystallization in 286 K, 51 nuclei are counted. In the second run with the 30 K/min rate, most of the crystallization occurs in the second stage, and the final number of nuclei is even larger, i.e., 72. The $N(T)$ plots for all cooling rates (Fig. 5a) show that the increase in the nucleation rate occurs below 300 K. The final number of developed nuclei decreases with decreasing cooling rate, as during slower cooling the crystallization degree below 300 K is already high and formation of new nuclei is less probable than for fast cooling. Two stages of crystallization are also noticeable in the temperature dependence of the crystallization degree X (Fig. 5b) and crystallization rate $\mathrm{d}X/\mathrm{d}t$ (Fig. 5c). As the separation of two crystallization processes is easier for the $\mathrm{d}X/\mathrm{d}t$ vs temperature plot, where they are visible as two maxima instead of two steps, (6) in temperature scale was used to fit the experimental data. The fitting results in Fig. 5b were then obtained by integration of the

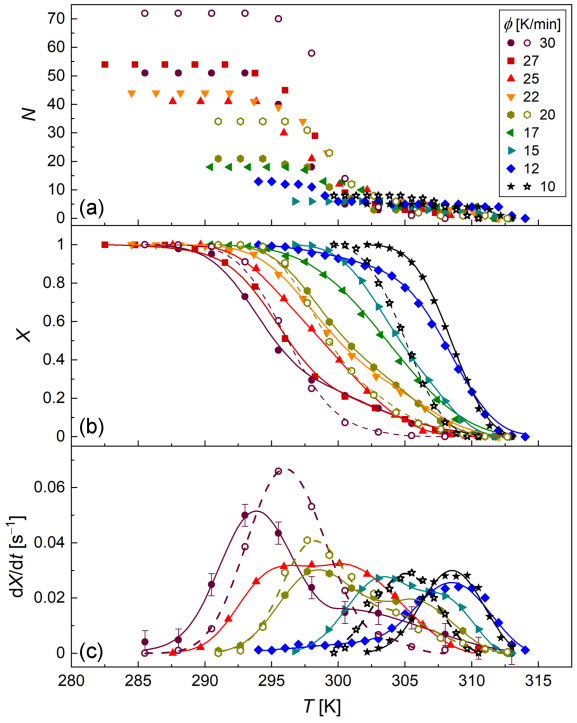

Fig. 5. Number of nuclei (a), crystallization degree (b), and crystallization rate (c) vs temperature during non-isothermal crystallization of 3F6FPhF6 for different cooling rates. For clarity, the uncertainty bars (0.01 for crystallization degree and 0.004 s^{-1} for crystallization rate) are drawn only for 30 K/min, and in the (c) panel only the results for representative cooling rates are shown. The lines are the fitting results of the Avrami model.

fitting results for crystallization rate. For 12 K/min, the beginning temperatures of both crystallization processes were fixed to be equal, $T_{01} = T_{02}$, because otherwise large uncertainties were obtained for some parameters. For 10 K/min and 17 K/min, only one crystallization process was clearly visible, thus (3) was fitted for one-step crystallization. The exponent n in all cases was fixed to 3, as it corresponds to the symmetric shape of the dX/dt vs temperature function for each crystallization process.

Next to the temperatures of the beginning of each step of crystallization, T_{01} and T_{02}, the characteristic temperatures determined by fitting (3) or (6) are the temperature T_{maxrate}, corresponding to the highest rate of crystallization, and $T_{X=0.9}$, which is the temperature where the degree of crystallization reaches 0.9. The latter temperature can be determined with more precision than the temperature at which the crystallization is completed. The T_{01}, T_{02}, and $T_{X=0.9}$ values for the cooling rates of 10–30 K/min are inserted into the so-called continuous cooling transition diagram [23, 24], which shows the relationship between the temperature and time during the experiment (Fig. 5). The beginning of cooling from 393 K was chosen as the moment when $t = 0$. Regardless of the cooling rate, the crystallization begins at roughly the same temperature; the T_{01} values are scattered around 313.5(7) K, while T_{02}, T_{maxrate}, and $T_{X=0.9}$ temperatures shift to lower values with the increasing cooling rate.

The kinetics of crystallization depends on two main factors: thermodynamic driving force, which influences nucleation, and diffusion rate, which influences crystal growth [25]. In the case of 3F6FPhF6, the crystallization process is investigated in temperatures above 280 K, therefore it can be assumed that the diffusion of molecules is fast enough not to hinder the crystallization, and the crystallization kinetics is controlled mainly by the rate of nucleation. It is confirmed by the increase in both the number of nuclei and the maximal crystallization rate with the decrease in temperature (Fig. 5). The thermodynamic driving force of crystallization is related to the difference in the free energy ΔG of the SmC^*_A and crystal phases, given by the approximate formula $\Delta G = (T_m - T)\Delta S_m$, where T_m is the melting temperature of a crystal phase, and ΔS_m is the entropy change upon melting [25]. The melting temperature of 3F6FPhF6 is $T_m = 335.8$ K, and the enthalpy change upon melting is $\Delta H_m = 32.2$ kJ/mol [14]. The corresponding entropy change can be obtained as $\Delta S_m \approx \Delta H_m/T_m = 69.1$ J/(mol K). The free energy ΔG increases with the lowering of the temperature, which facilitates the formation of stable nuclei. A decrease in temperature also corresponds to a decrease in the thermal energy of translational degrees of freedom. In the isotropic liquid state, there are three translational degrees of freedom, and according to the equipartition rule, they are related to the thermal energy equal to $3RT/2$, where R is the gas constant. In the smectic C^* and C^*_A phases, there are only two translational degrees of freedom — within the plane of smectic layers — because the molecules are unlikely to travel from one layer to another [26]. The $(T_m - T)\Delta S_m$ and $RT/2$ functions intersect at 317 K, if one includes the T_m and ΔS_m values of 3F6FPhF6, which is only a few degrees above the average T_{01} temperature. It suggests that when the thermodynamic driving force exceeds the thermal energy of one of the translational degrees of freedom, it "unlocks" the nuclei formation. The intersection of ΔG and RT occurs at 300 K, and below this temperature a rapid increase in the number of nuclei is observed. Thus, if ΔG exceeds the thermal energy of both translational degrees of freedom, it leads to a significant increase in the nucleation rate of 3F6FPhF6.

Although the vitrification of the SmC^*_A phase of 3F6FPhF6 was not observed, one can use the CCT diagram to estimate the cooling rate necessary to obtain the glassy liquid crystalline state in the sample [23, 24]. For 3F6FPhF6, it is unlikely to obtain the pure SmC^*_A glass because the first crystals are observed at ca. 314 K regardless of the cooling rate. However, one can consider the cooling rate neces-

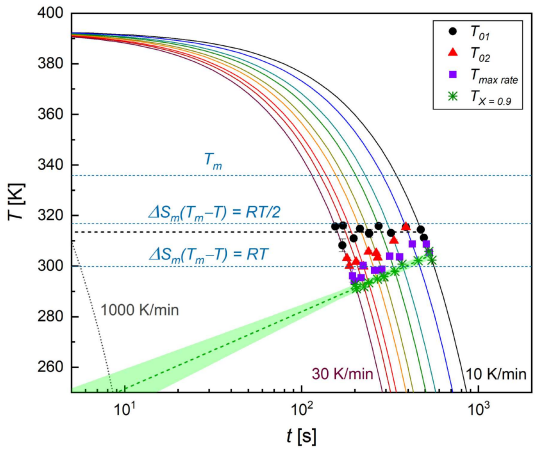

Fig. 6. Continuous cooling transition diagram of non-isothermal crystallization of 3F6FPhF6.

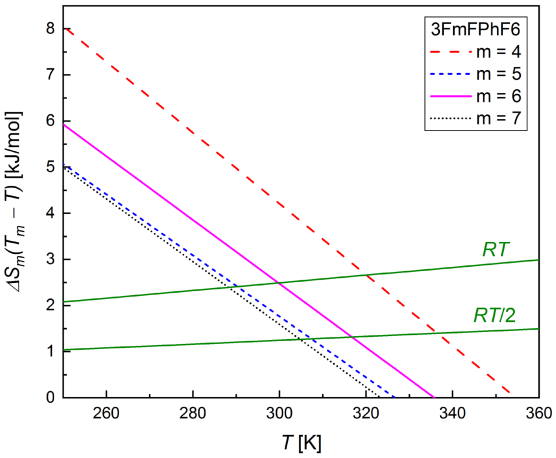

Fig. 7. Comparison of $\Delta G = (T_m - T)\Delta S_m$ [25], with thermal energy of two translational degrees of freedom within the smectic layers. The T_m and ΔS_m values were taken from [24].

sary to obtain at least a partially vitrified sample. The T_{02} and T_{maxrate} temperatures have a roughly linear dependence in the CCT diagram, but their values are too scattered for any extrapolations to higher cooling rates. The situation is different for $T_{X=0.9}$, which is very weakly scattered around the linear fit (Fig. 6) and therefore can be used for reliable extrapolation. The glass transition temperature T_g of 3F6FPhF6 is unknown, and instead, $T_g \approx 240$ K for the neighbor 3F5FPhF6 homologue [8] was used. It is assumed that T_g does not depend on the cooling rate because for 3F5FPhF6 no trend was observed [8]. The occurrence of crystallization exactly at T_g is unlikely due to the slowing of the molecular movements, and for 3F5FPhF6 crystallization was observed at no lower temperatures than about 10 K above T_g [8]. Taking it into account in the extrapolation made for 3F6FPhF6, one seeks the cooling rate for which the $T_{X=0.9}$ temperature is shifted down to 250 K. The estimated cooling rate is 1000 K/min, which is one order of magnitude higher than the rates applied in the experiment. Because of that, the uncertainty of this rate is significant, which is visualized by the 95% probability band drawn around the fitted line (Fig. 6). Note that 1000 K/min corresponds to the situation when the crystallization is stopped for the crystallization degree equal to 0.9, therefore, even for such fast cooling, 3F6FPhF6 is expected to crystallize in most of the sample volume.

To seek for causes why the 3FmFPhF6 homologues with $m = 4$, 6, 7 show a higher tendency to crystallization than that with $m = 5$, one can calculate at which temperatures the $\Delta G = (T_m - T)\Delta S_m$ function intersects with the thermal energy of one $(RT/2)$ and two (RT) translational degrees of freedom (Fig. 7). The T_m and ΔS_m values from [14] are used. The intersection points for $m = 4, 6$ are located at higher temperatures than for $m = 5$, which is in accordance with the observed slower crystallization for $m = 5$. However, for $m = 7$, the intersection points are located at an even slightly lower temperature than for $m = 5$, which does not agree with easier crystallization for $m = 7$. On the other hand, the thermodynamic driving force is only one of the factors contributing to the crystallization kinetics. The relationship between the structure of the crystal and the preceding SmC^*_A phase is also important [27], and at the same time, this contribution cannot be simply predicted. The crystal structures of 3FmFPhF6 compounds have not been solved yet, and even the arrangement of such types of molecules in the smectic phases is a matter of ongoing consideration [28]. Still, some structural differences in the SmC^*_A phase among 3FmFPhF6 homologues are visible in the temperature dependence of the helix pitch: for $m = 4, 5$ its value increases with increasing temperature, for $m = 6$, it is almost constant, while for $m = 7$, the decrease of helical pitch is reported [14]. The same changes in intra-molecular interactions, arising from changes in the -$\mathrm{C}_m\mathrm{H}_{2m}$- chain length, which lead to a different helical structure of the SmC^*_A phase, may also influence the formation of the crystal phase.

4. Conclusions

The smectic $\mathrm{C}^*_A \rightarrow$ crystal transition in the 3F6FPhF6 liquid crystal was investigated under the polarizing optical microscope under constant temperature conditions and during cooling with the 2–30 K/min rates. The degree of crystallization and number of nuclei were derived from the POM images. The intersection temperatures of the difference of the free energy between the smectic and crystal phases ΔG with the thermal energy of the translational degrees of freedom in the smectic phases were determined, and their impact on the crystallization process was underlined. The

nuclei formation was shown to occur faster when ΔG exceeded the RT value, contributing to two translational degrees of freedom, the third one hindered by the presence of the smectic layers. It was also shown, by comparison of the intersection temperatures obtained for other homologues from the 3FmFPhF6 series ($m = 4, 5, 7$), that not all differences in their crystallization tendency could have been explained by terms of the thermodynamic driving force. The structural relationship between the crystal and smectic C^*_A phase was presumed to be another cause of the observed difference in crystallization kinetics of the 3FmFPhF6 compounds. The interesting property observed for 3F6FPhF6 is a significant hysteresis of the SmC^*/SmC^*_A transition, which is shifted during cooling almost below the melting temperature of a crystal phase. Thanks to that, 3F6FPhF6, although it easily crystallizes in a pure form, may be considered as a component of liquid crystalline mixtures intended to exhibit the vitrified synclinic SmC^* phase instead of anticlinic SmC^*_A.

References

[1] J.L. Hutter, J. Bechhoefer, *J. Cryst. Growth* **217**, 332 (2000).

[2] T. Rozwadowski, M. Massalska-Arodź, Ł. Kolek, K. Grzybowska, A. Bąk, K. Chłędowska, *Cryst. Growth Des.* **15**, 2891 (2015).

[3] C.D. Syme, J. Mosses, M. González-Jiménez, O. Shebanova, F. Walton, K. Wynne, *Sci. Rep.* **7**, 42439 (2017).

[4] M. Jasiurkowska-Delaporte, T. Rozwadowski, E. Juszyńska-Gałązka, *Crystals* **9**, 205 (2019).

[5] A. Drzewicz, M. Jasiurkowska-Delaporte, E. Juszyńska-Gałązka, M. Gałązka, W. Zając, P. Kula, *Phys. Chem. Chem. Phys.* **23**, 17466 (2021).

[6] A. Deptuch, M. Piwowarczyk, M. Jasiurkowska-Delaporte, J. Kim, M. Urbańska, M. Skolarczyk, T. Jaworska-Gołąb, M. Marzec, *Crystals* **12**, 1028 (2022).

[7] A. Deptuch, E. Juszyńska-Gałązka, A. Drzewicz, M. Piwowarczyk, M. Urbańska, M. Tykarska, *Phase Trans.* **96**, 149 (2023).

[8] A. Deptuch, E. Juszyńska-Gałązka, M. Jasiurkowska-Delaporte, A. Drzewicz, M. Piwowarczyk, M. Urbańska, *Phase Trans.* **96**, 166 (2023).

[9] S. Lalik, A. Deptuch, P. Fryń, T. Jaworska-Gołąb, D. Dardas, D. Pociecha, M. Urbańska, M. Tykarska, M. Marzec, *Liq. Cryst.* **46**, 2256 (2019).

[10] A. Deptuch, A. Drzewicz, M. Dziurka, N. Górska, J. Hooper, T. Jaworska-Gołąb, E. Juszyńska-Gałązka, M. Marzec, M. Piwowarczyk, M. Srebro-Hooper, M. Tykarska, M. Urbańska, *Mater. Res. Bull.* **150**, 111756 (2022).

[11] P. Perkowski, Z. Raszewski, W. Piecek, K. Ogrodnik, M. Żurowska, R. Dąbrowski, X.W. Sun, *Mol. Cryst. Liq. Cryst.* **509**, 328/[1070] (2009).

[12] P. Morawiak, W. Piecek, M. Żurowska, P. Perkowski, Z. Raszewski, R. Dąbrowski, K. Czupryński, X.W. Sun, *Opto-Electron. Rev.* **17**, 40 (2009).

[13] M. Żurowska, R. Dąbrowski, J. Dziaduszek, K. Czupryński, K. Skrzypek, M. Filipowicz, *Mol. Cryst. Liq. Cryst.* **495**, 145/[1497] (2008).

[14] M. Żurowska, R. Dąbrowski, J. Dziaduszek, K. Garbat, M. Filipowicz, M. Tykarska, W. Rejmer, K. Czupryński, A. Spadło, N. Bennis, J.M. Otón, *J. Mater. Chem.* **21**, 2144 (2011).

[15] N. Osiecka, Z. Galewski, M. Massalska-Arodź, *Thermochim. Acta* **655**, 106 (2017).

[16] C.A. Schneider, W.S. Rasband, K.W. Eliceiri, *Nat. Methods* **9**, 671 (2012).

[17] M. Avrami, *J. Chem. Phys.* **7**, 1103 (1939).

[18] M. Avrami, *J. Chem. Phys.* **8**, 212 (1940).

[19] I. Avramov, K. Avramova, C. Rüssel, *J. Cryst. Growth* **285**, 394 (2005).

[20] N. Apiwanthanakorn, P. Supaphol, M. Nithitanakul, *Polym. Test.* **23**, 817 (2004).

[21] C.N. Velisaris, P. Supaphol, M. Nithitanakul, *Polym. Eng. Sci.* **26**, 1574 (1986).

[22] A. Drzewicz, E. Juszyńska-Gałązka, M. Jasiurkowska-Delaporte, P. Kula, *CrystEngComm* **24**, 3074 (2022).

[23] T. Rozwadowski, M. Jasiurkowska-Delaporte, M. Massalska-Arodź, Y. Yamamura, K. Saito, *Phys. Chem. Chem. Phys.* **22**, 24236 (2020).

[24] T. Rozwadowski, Y. Yamamura, K. Saito, *Cryst. Growth Des.* **21**, 2777 (2021).

[25] M.D. Ediger, P. Harrowell, L. Yu, *J. Chem. Phys.* **128**, 034709 (2008).

[26] G. Vertogen, W.H. de Jeu, *Thermotropic Liquid Crystals, Fundamentals*, Springer-Verlag, Berlin 1988.

[27] H. Tanaka, *J. Non.-Cryst. Sol.* **351**, 678 (2005).

[28] A. Deptuch, T. Jaworska-Gołąb, M. Dziurka, J. Hooper, M. Srebro-Hooper, M. Urbańska, M. Tykarska, M. Marzec, *Phys. Rev. E* **107**, 034703 (2023).